Extraction of trench geometry and linewidth of nanoscale grating targets in (110)-oriented silicon using angle-resolved scatterometry

Heather J. Patrick,[1,2] Thomas A. Germer,[2] Michael W. Cresswell,[2]
Bin Li,[3] Huai Huang,[3] and Paul S. Ho[3]

[1]*KT Consulting, Inc., Antioch, CA 94509 USA*
[2]*National Institute of Standards and Technology, Gaithersburg, Maryland 20899 USA*
[3]*Cockrell School of Engineering, University of Texas at Austin, Austin, TX 78712 USA*

ABSTRACT

The extraction of nanoscale dimensions and feature geometry of grating targets using signature-based optical techniques is an area of continued interest in semiconductor manufacturing. In the current work, we have performed angle-resolved scatterometry measurements on grating targets of 180 nm pitch fabricated by electron beam lithography and anisotropic wet etching of (110)-oriented silicon. The use of oriented silicon results in grating lines with nominally vertical sidewalls, with linewidths estimated by scanning electron microscopy (SEM) to be in the sub-50 nm range. The targets were designed to be suitable for both optical scatterometry and small-angle x-ray scattering (SAXS) measurement. As a consequence of the lattice-plane selective etch used for fabrication, the target trenches do not have a flat bottom, but rather have a wide vee shape. We demonstrate extraction of linewidth, line height, and trench profile using scatterometry, with an emphasis on modeling the trench angle, which is well decoupled from other grating parameters in the scatterometry model and is driven by the crystalline orientation of the Si lattice planes. Issues such as the cross-correlation of grating height and linewidth in the scatterometry model, the limits of resolution for angle-resolved scatterometry at the wavelength used in this study (532 nm), and prospects for improving the height and linewidth resolution obtained from scatterometry of the targets, are discussed.

Keywords: gratings, ellipsometry, optical critical dimension metrology, oriented silicon, reflectometry, rigorous coupled-wave, scatterometry

1. INTRODUCTION

Recent advances in semiconductor and micro-electro-mechanical systems (MEMS) processing have resulted in the ability to manufacture devices with features measured in tens of nanometers. These nanoscale features are pushing the limits of metrology tools, with solutions for sub-25 nm features becoming increasingly urgent. Scatterometry, a non-imaging optical technique, is expected to be a key technology in current and future semiconductor manufacturing processes as cited in the most recent edition of the International Technology Roadmap for Semiconductors.[1] Scatterometry, also referred to as optical critical dimension (OCD) scatterometry, is a model-based measurement method in which the characteristics of regular features (such as lines or holes) in a grating target are extracted by comparing a measured optical signature of the target to theoretically generated signatures using a library or regression algorithm.[2,3,4] The optical signature is not an image of the lines in the target, as the target features are often unresolvable by the wavelengths used, but is derived instead from reflectometry or ellipsometry of the illuminated lines in the target as a whole.

In the current work, we demonstrate the use of angle-resolved scatterometry, in which the optical signature consists of the polarized reflectance of a target at a single wavelength as a function of angle of incidence, to extract the line profile of nanoscale-width, high-aspect-ratio line grating targets fabricated in (110)-oriented silicon. Under particular conditions, lattice-plane-selective wet etching of (110) silicon produces lines with vertical, atomically flat sidewalls, a process that was developed for fabrication of critical-dimension reference standards.[5] By combining these techniques with electron-beam lithography, lines as narrow as 20 nm can be fabricated. Gratings consisting of these silicon nanolines

Instrumentation, Metrology, and Standards for Nanomanufacturing II, edited by Michael T. Postek, John A. Allgair,
Proc. of SPIE Vol. 7042, 70420B, (2008) · 0277-786X/08/$18 · doi: 10.1117/12.796286

have been recently used in studies of mechanical properties of silicon for nano-electro-mechanical systems (NEMS), where the rectangular cross section and high aspect ratio of the lines were shown to produce superb mechanical properties.[6] The gratings in the current study had linewidths (as measured by SEM) estimated to be in the 25 nm to 50 nm range, heights of around 500 nm, and were designed to be suitable for both scatterometry and small-angle x-ray scattering (SAXS) measurements, allowing future comparisons of the two techniques. In addition, the question of scatterometry sensitivity for features with widths in the tens of nanometers has been of recent interest. A recently completed theoretical study of the expected resolution of different types of scatterometry tools to dimensional changes in nanoscale targets representing typical amorphous silicon gate gratings as well as resist gratings indicates this resolution will be dependent on both the target geometry and materials, and the type of scatterometry data that is used.[7] Here, we explore the experimental and theoretical sensitivity of angle-resolved scatterometry for silicon nanoline targets.

2. GRATING FABRICATION

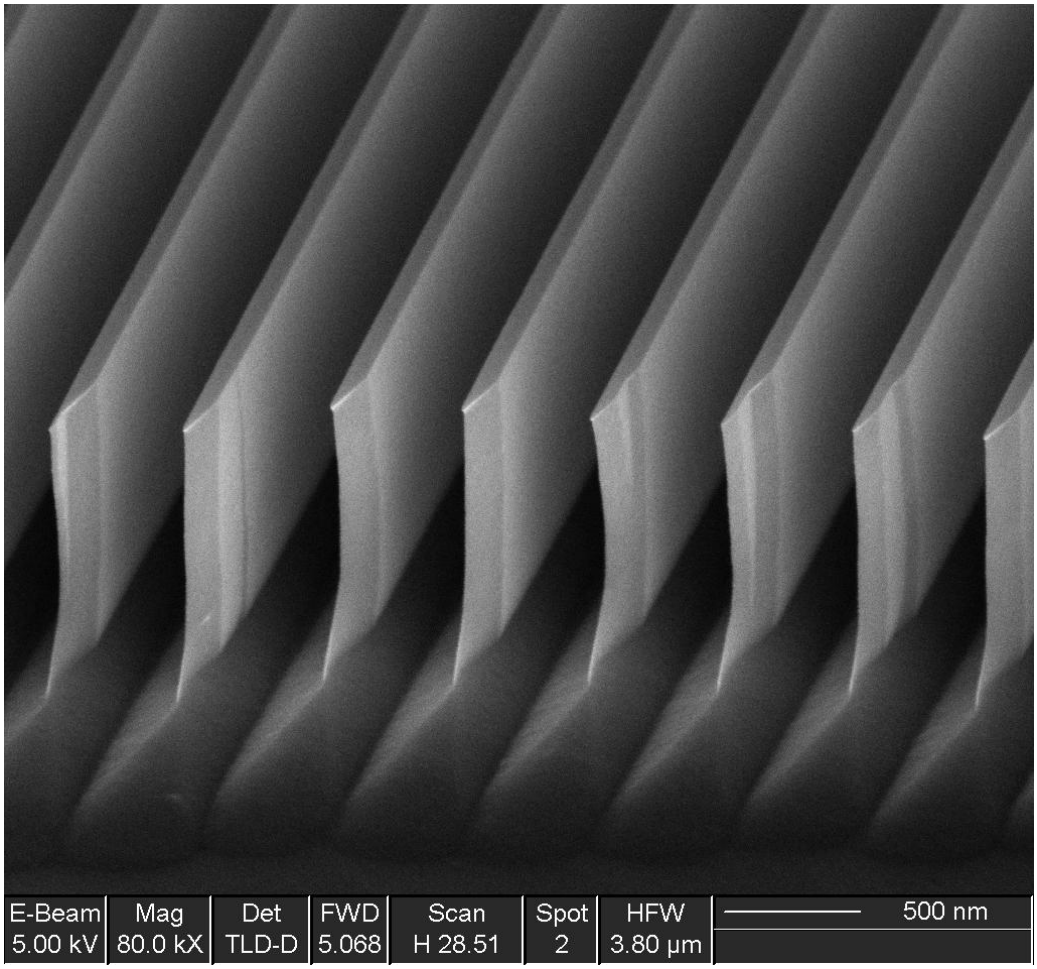

FIG. 1 SEM image of a typical Si nanograting, taken in cross section with a 55° tilt angle. The vertical sidewalls, high aspect ratio, and angled trench bottom surfaces are evident.

The silicon nanoline targets were fabricated by electron beam lithography (EBL) associated with anisotropic wet etching of (110)-oriented silicon.[6] The fabrication process began with chemical vapor deposition of an oxide layer on a Si (110) wafer followed by the deposition of a thin Cr layer. A positive-tone resist was spun onto the wafer and patterned using an electron beam exposure system. Pattern transfer from the resist was performed by plasma etching of the chromium and oxide down to the silicon surface. Subsequently, the residual resist was removed, and tetra-methyl-ammonium hydroxide (TMAH) was used for anisotropic etching of the Si, with the remaining chromium and oxide layers as the

hard mask. When the EBL patterned lines were aligned along one of the <112> directions on the Si surface, parallel Si lines were produced by the anisotropic etching along the {111} crystalline planes, which had vertical and atomically-flat sidewalls. Finally, the residual Cr and oxide were removed by a Cr etchant and a buffered oxide etchant (BOE).

Four arrays of grating targets, referred to as arrays S1–S4, were investigated in the current study. An individual grating target measured 60 μm × 60 μm. For the current study, we investigated the target in each array that was best-aligned to a <112> direction of the Si surface. The grating pitch was 180 nm, and the linewidths of the best-aligned target in each array were estimated by using top-down SEM to vary from 25 nm (for the S4 target) to 51 nm (for the S1 target). Figure 1 shows a perspective view near one end of the Si lines for a representative nanograting target, where a section of the grating was etched specifically for the purpose of SEM imaging. This particular target has a pitch of 450 nm, in order to aid in viewing the line and trench geometry. The high crystal quality and well-defined line geometry, along with the atomically flat sidewalls and narrow linewidths, can be seen in the figure. It is also apparent the trenches do not have a flat bottom, but rather have a wide vee shape bottom due to the lattice-plane selective wet etching. A similar trench shape was observed in cross-section images taken at the edges of targets from the S1-S4 arrays used in this study. The orientation of the faces of the vee was estimated from the SEM image to be tilted by about 30° from horizontal. This trench angle is expected to be fixed by the crystallography of the silicon lattice, but was also included as a variable in the scatterometry model. Using the trench angle extracted from scatterometry and the SEM image, we make a tentative identification of the lattice plane of this surface (see below).

3. DATA ACQUISITION

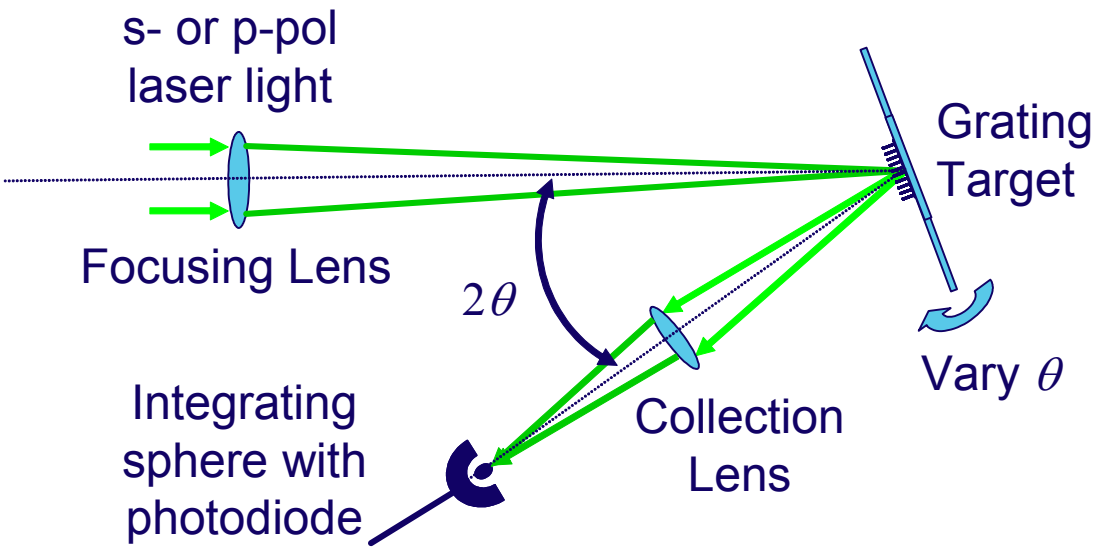

FIG. 2. Orientation of incident beam, target, and detector when collecting specular reflectance scatterometry signatures. The incident laser beam is focused to a roughly 15 μm spot size at the target, and the incident angle was scanned over a range of 10° to 40°.

Data was obtained using the NIST Goniometric Optical Scatter Instrument (GOSI). GOSI is a general-purpose research instrument for making laser-based scattering measurements at wavelengths from 266 nm to 633 nm.[8] In the current work, we use GOSI for angle-resolved scatterometry, making in-plane measurements of the specular reflectance of a grating target for s- and p-polarizations, over a range of angles of incidence. However, the instrument has the flexibility for full hemispherical scattering measurements at nearly any combination of incidence and scattered angles, with multiple detector types providing a wide dynamic range for low light scattering applications. In addition to scatterometry, GOSI applications include nanoscale particle sizing and characterization of surface- and sub-surface roughness of unpatterned samples.[9,10] Recent upgrades have increased the maximum sample size to that of a 300 mm wafer, increased its maximum angle of incidence to 80°, achieved micrometer-scale repeatability of target positioning, and extended the operating wavelength to 266 nm.

The scatterometry measurement setup used in GOSI for this work is shown in Fig. 2. Light from a 532 nm laser is incident on a grating target at a variable angle of incidence θ. The light is focused on the target to a roughly gaussian spot with a 15 μm $1/e^2$ beam diameter.[11] The laser polarization is set at either p- (electric field in the plane of incidence) or s- (electric field perpendicular to the plane of incidence) polarization. A small portion of the beam is picked off before the final focusing lens to provide a reference intensity measurement, so that the absolute reflectance can be measured. The detector angle is maintained at twice the angle of incidence (2θ) so that the specular component of the grating reflectance is collected, and θ is varied over a range from 10° to 40°. While GOSI supports increasing the range of angle of incidence up to 80°, the spot size increases with angle due to geometric effects. Restricting the incidence angle to 40° and below insured that the incident spot remained around 20 μm or less over the full measurement range.

4. MODELING

The theoretical optical signatures are obtained using the rigorous coupled wave (RCW) analysis for surface relief gratings developed by Moharam *et al,*,[12,13] with a modification suggested by Lalanne and Morris[14] to improve the convergence of the calculations. This method solves the electromagnetic problem for a plane wave incident upon a medium having a dielectric function, $\varepsilon(x,y,z) = \varepsilon_k(x)$, which is periodic in *x*, independent of *y*, and independent of *z* within each of a finite number of layers, indicated by index *k*. The solution requires Fourier series expansions of $\varepsilon_k(x)$ and $1/\varepsilon_k(x)$ for each layer. In practice, the Floquet expansions of the fields are truncated at some maximum order *M*; for the current targets *M* was chosen to be 20. The code implemented by NIST for generating theoretical signatures is publically available.[15]

Figure 3 shows the line profile used in modeling the targets Initial modeling was attempted using a flat trench bottom; however, the fits were poor and indicated non-physical height variations between targets of the various arrays. The model includes grating pitch, which was well-known and thus fixed at p = 180 nm, and a layer of native oxide, which was also held fixed at t = 2 nm. The floating parameters were line height h, linewidth w, and trench bottom angle, q. Values for the optical constants of the silicon and native oxide at the measurement wavelength of 532 nm were taken from the literature,[16] and were also held fixed in the model.

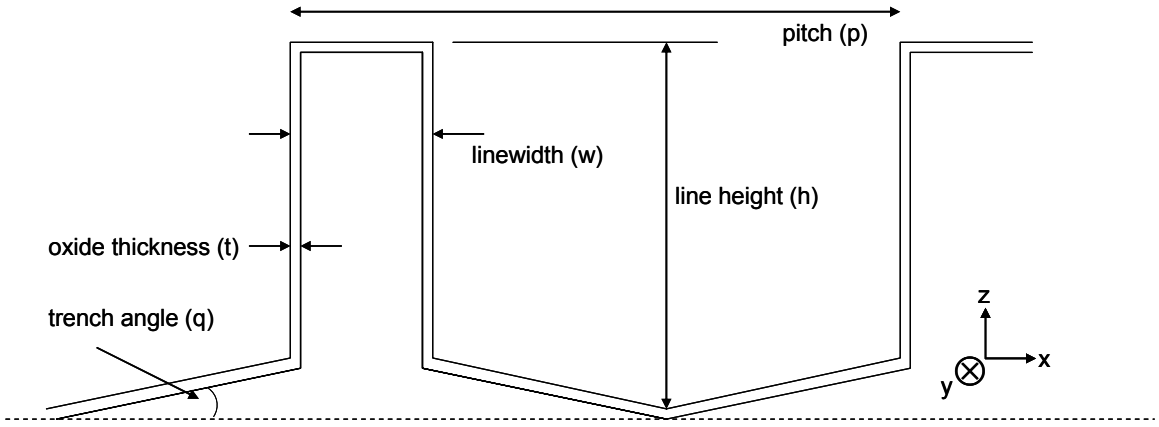

FIG. 3. The line profile model used for RCW modeling of scatterometry signatures of the grating targets. This diagram is not to scale.

In order to understand the model sensitivity to the parameters of the line profile model, we generated expected optical signatures versus variation in height, width, and trench angle. For each simulation, angle-resolved spectra were generated from theory versus a change in any one of these parameters, while the other parameters were held constant. Figure 4 shows the results of these simulations. The nominal parameter values were h = 490 nm, w = 35 nm, and q = 30°.

Figure 4 demonstrates several important points about the expected sensitivity of the current scatterometry measurement. First, from comparing Fig. 4(a) and Fig. 4(b), it is seen that significant cross-coupling between line height and linewidth exists for the conditions of our measurement. Changes in these two parameters cause similar effects on the s-polarized reflectance, while making minor changes (but in the same direction, decreasing for increasing h or w) in the p-

polarized reflectance. Thus it will be difficult to distinquish changes in width from changes in height from angle-resolved scatterometry at this optical wavelength and angle range. Changes in the third parameter, the trench angle q, however (Fig. 4c)), cause similar magnitude changes in both the s- and p-polarized reflectance, and additionally the s-polarized reflectance increases with increasing q, while the p-polarized reflectance decreases. This suggests we should be able to extract the trench angle from the scatterometry data. We can also estimate the relative sensitivity of the reflectance measurement to changes in the parameters. While a 1 nm change in linewidth, for example, causes large changes in reflectance, a several degree change in trench angle is required to show a similar magnitude of change.

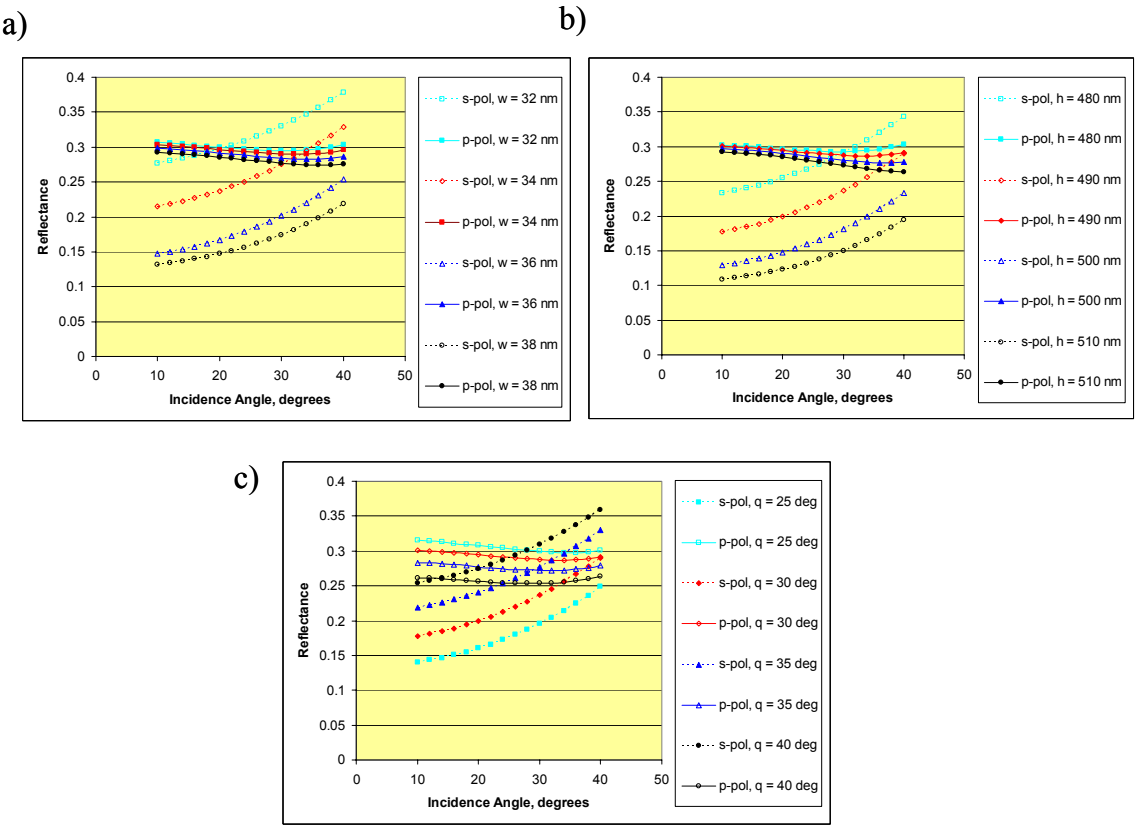

FIG. 4. Theoretical sensitivity of s- and p-polarized reflectance as (a) linewidth, w, is varied while other parameters are held constant, (b) line height, h, is varied with other parameters constant, and (c) bottom trench angle, q varied while other parameters held constant. The nominal parameter values were h = 490 nm, w = 35 nm, and q = 30°. The pitch p was 180 nm for all simulations, and the oxide thickness t was 2 nm.

In order to determine the best fit parameters for each target, a theoretical library of optical signatures that encompassed all of the expected range of the grating parameters, over the fabrication conditions of the targets in the S1 through S4 arrays, was generated. For the library, h was varied over a range from 480 nm to 540 nm in 5 nm steps, w was varied from 20 nm to 50 nm in 0.5 nm steps, and q was varied from 20° to 40° in 1° steps. Because the theoretical signatures are quite smooth in angle of incidence θ, the model was generated in 5° steps from θ = 10° to θ = 40° and the results were interpolated for other angles. To determine the best fit theoretical signature to a given measured optical signature, we compared the theoretical signatures from the library to the data and minimized the following figure of merit (FOM):

$$\chi_r^2 = \frac{1}{(2N-\nu)} \sum_{i=s,p} \sum_{j=1}^{N} \left(\frac{R_{meas,i}(\theta_j) - R_{th,i}(\theta_j)}{\sigma_i(\theta_j)} \right)^2 \qquad (1)$$

where N = 16 is the number of discrete angles j where the reflectance was measured, ν is the number of adjustable parameters used when generating the theoretical reflectance signatures, and the subscript i is used to denote that both s-

and p-polarization reflectances are included simultaneously when calculating χ^2_r. Inside the summation, $R_{meas,i}(\theta_j)$ is the measured reflectance for the polarization i at the angle θ_j, $R_{th,i}(\theta_j)$ is the theoretical reflectance for the polarization i at the angle θ_j, and $\sigma_i(\theta_j)$ is the estimated uncertainty in the measured reflectance for the polarization i at the angle θ_j. This equation is the reduced-χ^2, which is used as a relative measure of goodness-of-fit for different parameter sets. The parameter set with the smallest χ^2_r is gives the best estimate h, w, and q for that target, within the limits of the theoretical line profile model that was chosen.

5. RESULTS AND DISCUSSION

5.1. Line profile parameters extracted from scatterometry

Figure 5 shows the measured and modeled reflectance signatures for the target estimated to have the best alignment to the silicon lattice planes during electron beam writing, for each target array S1 – S4. The parameters for each best fit theoretical signature are shown in the figure. Also shown in the figure are the target linewidths independently measured from top-down SEM images of the targets. Values of χ^2_r for the best fit signature ranged from 0.35 (for the S3 target) to 1.9 (for the S4 target), as shown.

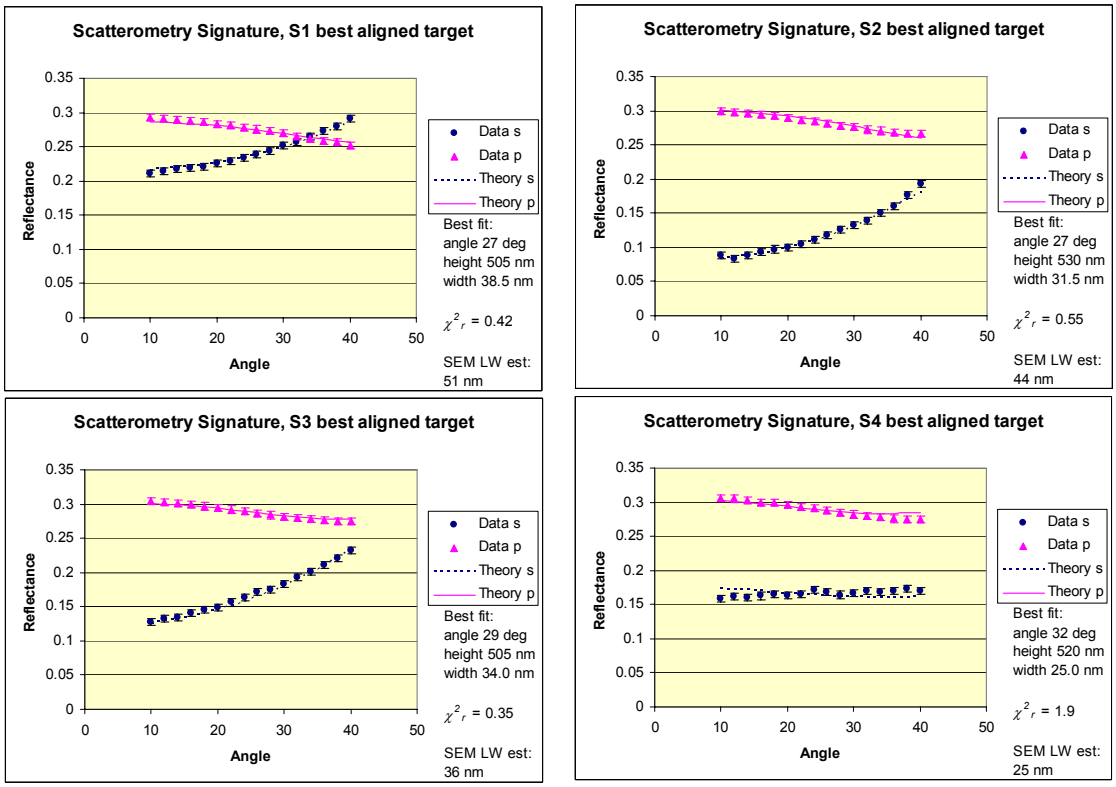

FIG. 5. Measured s- and p- reflectance spectra (s-pol, circles, p-pol, triangles) along with final best fit theory (lines), taken from the comparing reflectance spectra for the best-aligned targets in the S1 – S4 grating arrays with the theoretical library described in the text. Parameters from the best fit theoretical spectra are shown on each graph, along with an independent estimate of the target linewidth taken from a top-down SEM image.

The fits for these four targets highlight some successes, as well as some difficulties, for the current model and scatterometric technique. The fits to the data are generally good, and fall within the estimated uncertainty in reflectance of 0.005 (1-σ). The extracted trench angle, which varies from 27° to 32° for these targets, is reasonably consistent from target to target, as expected from the silicon crystallography. The heights, which range from 505 nm to 530 nm, are

within range of the 490 nm ± 10 nm measured by SAXS.[17] However, while the linewidth for the targets shows the same general trend as the SEM measurements, the S2 and S3 targets are interchanged. We might also expect better consistency in height and trench angle, as these parameters were expected to be constant over the range of fabrication conditions used.

In the data and best fits to the model shown in Fig. 5, the χ^2_r is less than 1 in some cases (a "good fit" is generally expected to have $\chi^2_r \approx 1$).[18] This indicates we may have somewhat overestimated the signal error. However, we also see some systematic deviations of the data from the model, particularly in the case of the S4 target. As is typical in scatterometry, the presence of significant systematic errors between data and theory make an objective determination of goodness of fit, and thus a statistically meaningful determination of the uncertainty in the extracted parameters, difficult.[18,19] Even so, we can look at the distribution of χ^2_r over the library parameter space to observe correlations in parameters and relative confidence levels in the parameters. Theoretical signatures in the library that produce similar values of χ^2_r are all equally reasonable fits to the data. To demonstrate the range of height and width values that produce similar data fits to the best-aligned target of the S1 array, in Fig. 6 we have plotted all combinations of height and width that (along with any trench angle) resulted in $\chi^2_r \leq 1.3$. Following Ref. 18, it can be shown that for the values of N and ν in Eq. 1, this is the range of 3-σ correlated uncertainty (i.e., the 99% confidence level) for fitting two parameters simultaneously, when the minimum χ^2_r is a statistically good fit with $\chi^2_r = 1$. In the current case, where the minimum χ^2_r for the dataset is 0.42 and the errors between the data and the model are systematic in nature, rather than strictly statistical, this interpretation is not completely rigorous. However, it does serve to demonstrate that the confidence ellipse for height and width is long and narrow, illustrating the difficulty in independently extracting height and width for these targets using the existing scatterometry data set.

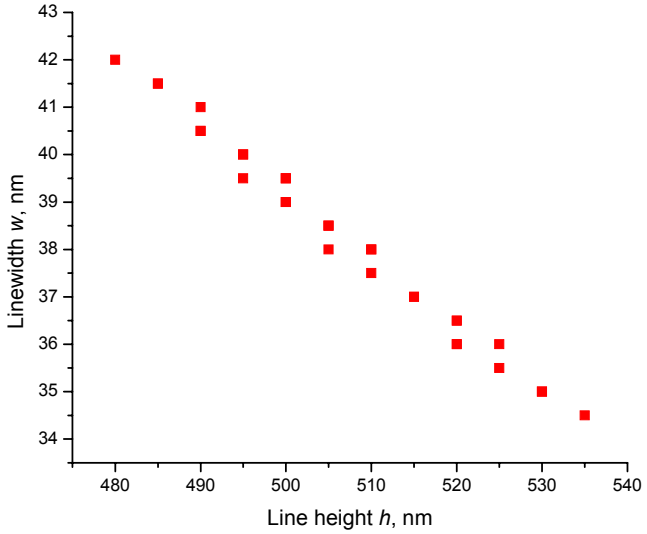

FIG. 6. Cross-coupling of linewidth, w, and line height, h, for fits of the experimentally obtained dataset from the best-aligned target in the S1 array to the theoretical library described in Section 4. The plotted points represent all combinations of h and w from the theoretical library that resulted in a $\chi^2_r \leq 1.3$ as defined by Eq. 1.

While the current scatterometric technique and the line profile model chosen have some limitations in terms of cross-correlations between parameters as described above, there may also be limitations imposed by the targets themselves, and by the other metrologies used to characterize them. For example, while efforts were taken to choose targets that were best aligned to the silicon lattice planes, linewidth or line edge roughness was observed in some SEM images of the targets, particularly in the smallest linewidth, S4 array. This effect is not included in the model, which assumes an infinite array of identical lines. There is also evidence from SAXS that within each grating target, the linewidths of the nanolines within about 10 μm of the edge of the target are considerably larger than those at the center, and that the center lines may be narrower than our current SEM and scatterometry linewidth estimates shown in Fig. 5.[17] The spatial non-

uniformity of the linewidths is attributed to the EBL proximity effect, in which areas in the central region of a pattern receive higher total dosage than the border region. While we have attempted to restrict the scatterometry data collection to a small area at the center of each target, where the lines were expected to be the most uniform, it is possible that the extracted scatterometry linewidths shown in Fig. 5 are influenced by reflection from the wider lines at the perimeter of the target. Ideally, this nonuniformity should be eliminated as much as possible before attempting more rigorous comparison of scatterometry, SEM, and SAXS results. It can also be difficult to make accurate SEM measurements for very small linewidths due to charging effects, an effect which may have played a role in the accuracy of the SEM estimates shown in Fig. 5. While we expect the trend of decreasing linewidth with increasing array number shown by the SEM measurements to be correct, it is conceivable that the linewidths of the S2 and S3 targets are nearly the same or even interchanged, as indicated from scatterometry. Finally, the scatterometry measurement is made over at least a 20 μm region over the center of the target, while the SEM images generally included a region extending 2 μm or less. Depending on the locations of the SEM images within the targets and the magnitude of the EBL proximity effects, there could be differences between the linewidths sampled by the SEM and by the scatterometer. Investigations of these limitations are ongoing.

5.2. Comparison of extracted trench angle with expected crystalline silicon etch planes

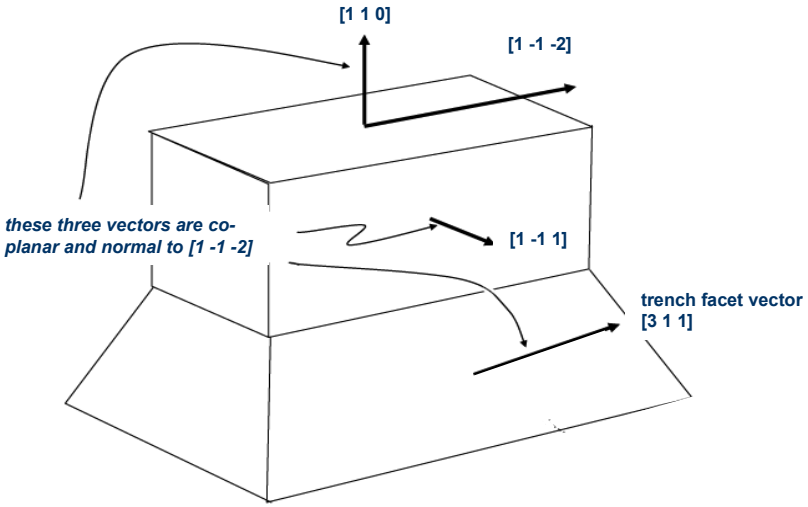

FIG. 7. Directions of the crystallographic planes for the silicon nanolines.

From the scatterometry data of the four best-aligned targets presented in Fig. 5, we have estimated the trench angle q to be in the range of 27° to 32°. These results are consistent with those obtained from the SEM image in Fig. 1. We now turn to identification of the crystal plane most like associated with this trench angle. For these samples, the surface normal is in the {1 1 0} family of planes, while the vertical sidewalls of the etched lines are {1 1 1} planes. The intersection of the {1 1 0} plane with the {1 1 1} planes are lines in the <1 1 2> family of vectors. If we follow the convention of Cresswell et al.,[20] then, as shown in Fig. 7 for (1 1 0) oriented silicon, the silicon wafer surface normal is in the direction [1 1 0], and the direction along the lines as shown is given by [1 -1 -2], while the direction perpendicular to the line surface is [1 −1 1]. We wish to find the facet vector for the angled trench bottom, where the facet vector must be perpendicular to the [1 -1 -2] direction of the lines. Any crystal plane containing [1 -1 -2] must have a facet vector

$$n*[1 \quad 1 \quad 0]+m*[1 \quad -1 \quad 1] \tag{2}$$

where n and m are integers. Using the expression for the angle θ between two vectors $\boldsymbol{a}$ and $\boldsymbol{b}$

$$\theta = \cos^{-1}[(\mathbf{a}\cdot\mathbf{b})/(|\mathbf{a}||\mathbf{b}|)], \tag{3}$$

we find that the facet vector [3 1 1] (n = 2 and m = 1) is the lowest index vector with an angle close to 30°. The angle between the facet vector [3 1 1] and the surface normal [1 1 0] (which is the same angle as the trench angle q shown in Fig. 3) is 31.5°. The family of vectors containing [3 1 1] has been identified as an anisotropic-etch stable plane of silicon,[21] and is in the range of the angle estimated from scatterometry and the SEM image. It is reasonable to identify the trench bottom surface with the [3 1 1] vector normal.

6. ANALYSIS OF ALTERNATIVE SCATTEROMETRIC TECHNIQUES

One of the limitations of the current set of scatterometric data is the relatively long wavelength (relative to the grating pitch of 180 nm) of the 532 nm laser, and the cross-coupling of parameters, which makes the independent assessment of height and width difficult. However, in addition to the angle-scanning technique used here, there are other variations of signature-based optical tools that can provide scatterometry data, including spectroscopic ellipsometry, spectroscopic reflectometry, angle scanning at different optical wavelengths, and others. We have recently implemented a statistical analysis of the RCW code that can identify the expected uncertainty in parameters of a grating model, given the optical tool, measurement modality, and expected uncertainty in the signature provided by that tool.[7] Based on the methods of Ref. 18, this software calculates the variation in optical signature brought about by changes in the different parameters (height, width, sidewall angle, etc.) of the grating model, and generates the χ^2-distribution in this multi-dimensional parameter space. From this distribution, we can find the range of grating parameters that yield statistically equivalent measurements, and extract the expected 3-σ uncertainty in each parameter.

Based upon our previous work, which indicated advantages in spectroscopic scanning and/or angle scanning at shorter wavelengths for extracting the parameters of certain grating profiles,[7] we investigated the theoretical sensitivities of three tools for the nanoline grating profile shown in Fig. 3. Tool A is our current angle scanning experiment, run at a wavelength of 532 nm. Tool B is polarized spectroscopic reflectometry at normal incidence, with a scanning wavelength range of 250 nm to 950 nm. Tool C is angle scanning at a wavelength of 266 nm. The tools are summarized in Table 1. It should be noted that we have held the number of points in the scatterometry signature and the noise level (which was 0.005 in the reflectance) fixed across the three tools in order to make a comparison for the noise signature estimated in the current experimental data. However, it is unlikely that real tools would be run in this manner. In particular, the spectroscopic scan would generally be done at many more wavelengths, which would be expected to improve its sensitivity.

Tool	Measurement	Wavelength	Angle of incidence	Number of angle or wavelength steps	Noise
A	s- and p-pol reflectance vs. angle	532 nm	10 to 40 degrees	32	0.005
B	s- and p-pol reflectance vs. wavelength	250 nm to 950 nm	0 degrees	32	0.005
C	s- and p-pol reflectance vs. angle	266 nm	10 to 40 degrees	32	0.005

Table 1. Overview of the three optical tools used in the sensitivity simulations.

There are many subtleties involved in simulations of scatterometric sensitivity, but we will here concentrate on parameter sensitivity when the model allows the three parameters of height, width, and trench angle to be floating parameters to be extracted from the model, and the oxide thickness parameter to be a parameter that is considered to be known, but with a fixed uncertainty. The pitch is considered fixed and known exactly at 180 nm. Because the optical signature in general exhibits nonlinear changes with changes in the parameter values, all simulations were done at the nominal values for the floating parameters of h = 500 nm, w = 35.5 nm, q = 30°. The fixed thickness parameter was taken to be t = 2.0 nm ± 0.3 nm.

	3-σ uncertainty in parameter		
Tool	linewidth, w, nm	line height, h, nm	trench angle, q, degrees
A	1.59	7.40	0.76
B	0.65	2.21	0.78
C	0.50	2.21	0.96

Table 2. Theoretical limits to 3-σ uncertainties in floating parameters linewidth, line height, and trench angle, for the three optical tools described in Table 1 and the assumptions described in the text.

Table 2 shows the results for the expected uncertainty in the floating parameters of linewidth, line height, and trench angle for the three tools. We could expect significant improvements in linewidth and especially line height sensitivity by moving to a spectroscopic measurement, or to a short wavelength angle-resolved measurement, if the same uncertainty in the optical signature as in the present experiment could be maintained. It should also be noted, however, that in the results of Table 2, a significant part of the total parameter uncertainty for all of the tools comes from the fixed uncertainty in the oxide thickness, *t*. This is unfortunate when considering the comparison of scatterometry linewidth from such a target to the linewidth measured by atomic force microscopy (AFM) , for example. While the AFM measures the full width including the oxide layer, the uncertainty in the scatterometrically measured linewidth will be highly dependent on the knowledge of the thickness of the native oxide layer. Since this layer is formed over time by exposure to air, it may be difficult to identify the layer thickness at the time of measurement to the 0.3 nm level we have specified. Finally, the theoretical uncertainties shown in Table 2 assume that the scatterometry dataset has statistically limited noise with no systematic errors, no uncertainty in the grating material optical constants, and an infinite, spatially uniform grating. In real systems, these limits may be as important or more important than the intrinsic sensitivity of the scatterometry tool to the grating model.

7. SUMMARY AND CONCLUSIONS

In this paper, we have given an overview of our initial scatterometric analysis for nanoline targets fabricated in (110)-oriented silicon. We have developed a line profile model that gives good fits to the experimental angle-resolved scatterometry data, and allows extraction of line height, linewidth, and the angle of the vee trench bottoms. The sensitivity of the scatterometry model to trench angle enables us to tentatively identify the trench bottom faces as {311} planes, which are known anisotropic-etch stable planes of silicon. While the cross-coupling of height and width in the current data set complicate the independent extraction of these parameters, the heights and widths extracted for the four targets investigated are within range of those expected from SAXS and SEM metrologies. We have also presented a theoretical analysis of the sensitivity of different types of scatterometric data to the line profile model, and conclude that improved height and width values could be obtained by using spectroscopic techniques or by using angle-resolved scatterometry at 266 nm. We anticipate that improvements in the target linewidth uniformity, more complete characterization of the targets through reference metrologies, and careful selection of the scatterometry technique will enable a more thorough comparison of scatterometry with other measurement methods for future silicon nanoline targets.

ACKNOWLEDGEMENTS

We thank the NIST Office of Microelectronics Programs for supporting this work, and acknowledge the use of the NIST Raritan cluster computing system.

REFERENCES

1. http://www.itrs.net/Links/2007ITRS/2007_Chapters/2007_Metrology.pdf
2. C.J. Raymond, M.R. Murnane, S.L. Prins, S.S.H. Naqvi, and J.R. McNeil, "Multiparameter grating metrology using optical scatterometry," J. Vac. Sci. Technol. B **15**, 361-368 (1997).
3. A. Levy, S. Lakkapragada, W. Mieher, K. Bhatia, U. Whitney, and M. Hankinson, "Spectroscopic CD Technology for Gate Process Control," *The 2001 IEEE Semiconductor Manufacturing Symposium,* 141-144 (2001).

4. W. Yang, J. Hu, R. Lowe-Webb, R. Kohlahalli, D. Shivaprasad, H. Sasano, W. Liu, and D.S.L. Mui, "Line-Profile and Critical-Dimension Monitoring Using a Normal Incidence Optical CD Metrology," IEEE Trans. on Semiconductor Manufacturing **17**, 564-572 (2004).
5. M.W. Cresswell, W.F. Guthrie, R.G. Dixson, R.A. Allen, C.E. Murabito, and J.V. Martinez de Pinillos, "RM 8111: Development of a Prototype Linewidth Standard," J. Res. Of the N.I.S.T. **111**, 187-203 (2006).
6. B. Li, M.K. Kang, K. Lu, R. Huang, P.S. Ho, R.A. Allen, and M.W. Cresswell, "Fabrication and Characterization of Patterned Single-Crystal Silicon Nanolines," Nano Letters **8**, 92-98 (2007).
7. R. Silver, T. Germer, R. Attota, B.M. Barnes, B. Bunday, J. Allgair, E. Marx and J. Jun, "Fundamental Limits of Optical Critical Dimension Metrology: A Simulation Study," in *Metrology, Inspection, and Process Control for Microlithography XXI*, Chas N. Archie, Ed., Proc. SPIE **6518**, 65180U-1-17 (2007).
8. http://physics.nist.gov/lag
9. T.A. Germer and C.C. Asmail, "Polarization of light scattered by microrough surfaces and subsurface defects," J. Opt. Soc. Am. A **18**, 1326-1332 (1999).
10. T.A. Germer, G.W. Mulholland, J.H. Kim, and S.H. Ehrman, "Measurement of the 100 nm NIST SRM® 1963 by laser surface light scattering," in *Advanced Characterization Techniques for Optical, Semiconductor, and Data Storage Components*, A. Duparré and B. Singh, Eds., Proc. SPIE **4779**, 60-71 (2002).
11. A.E. Siegman, *Lasers,* Mill Valley, University Science Books, 664, 1986.
12. M.G. Moharam, E.B. Grann, D.A. Pommet, and T.K. Gaylord, "Formulation for stable and efficient implementation of the rigourous couple-wave analysis of binary gratings," J. Opt. Soc. Am. A **12**, 1068-1076 (1995).
13. M.G. Moharam, D.A. Pommet, E.B. Grann, and T.K. Gaylord, "Stable implementation of the rigourous coupled-wave analysis for surface-relief gratings: enhanced transmitance matrix approach," J. Opt. Soc. Am. A **12**, 1077-1086 (1995).
14. P. Lalanne and G.M. Morris, "Highly improved convergence of the coupled-wave method for TM polarization," J. Opt. Soc. Am. A **13**, 779-784 (1996).
15. SCATMECH: Polarized Light Scattering Library, available at http://physics.nist.gov/Divisions/Div844/facilities/scatmech/html/index.htm
16. C.M. Herzinger, B. Johs, W.A. McGahan, J.A. Woolam and W. Paulson, "Ellipsometric determination of optical constants for silicon and thermally grown silicon dioxide via a multi-sample, multi-wavelength, multi-angle investigation," J. Appl. Phys. **83**, 3323-3336 (1998).
17. Chengqing Wang and Wen-li Wu, private communication.
18. W.H. Press, S.A. Teukolsky, W.T. Vetterling, and B.P. Flannery, *Numerical Recipes in C,* 2nd ed., Cambridge, United Kingdom: Cambridge University Press, 689-699, 1992.
19. H.J. Patrick and T.A. Germer, "Progress towards traceable nanoscale optical critical dimension metrology in semiconductors," in *Advanced Characterization Techniques for Optics, Semiconductors, and Nanotechnologies III*, A. Duparré, B. Singh, and Z.H. Gu Eds., Proc. SPIE **6672**, 66720L-1-9 (2007).
20. M.W. Cresswell, J.J. Sniegowski, R.N. Ghoshtagore, R.A. Allen, W.F. Guthrie, A.W. Gurnell, L.W. Lindholm, R.G. Dixson and E.C. Teague, "Recent developments in electrical linewidth and overlay metrology for integrated circuit fabrication process," Jpn. J. Appl. Phys. **35**, 6597-6609 (1996).
21. J.M. Lysko, "Anisotropic etching of the silicon crystal-surface free energy model," Materials Science in Semiconductor Processing **6**, 235-241 (2003).